Supercurrent-induced spin switching via indirect exchange interaction

Chi Sun and Jacob Linder

Center for Quantum Spintronics, Department of Physics, Norwegian University of Science and Technology, NO-7491 Trondheim, Norway

(Received 13 October 2023; revised 20 May 2024; accepted 22 May 2024; published 5 June 2024)

Localized spins of single atoms adsorbed on surfaces have been proposed as building blocks for spintronics and quantum computation devices. However, identifying a way to achieve current-induced switching of spins with very low dissipation is an outstanding challenge with regard to practical applications. Here, we show that the indirect exchange interaction between spin impurities can be controlled by a dissipationless supercurrent. All that is required is a conventional superconductor and two spin impurities placed on its surface. No triplet Cooper pairs or exotic material choices are needed. This finding provides a new and accessible way to achieve the long-standing goal of supercurrent-induced spin switching.

DOI: 10.1103/PhysRevB.109.214409

I. INTRODUCTION

Electrical manipulation of spin or magnetization is crucial in the development of spintronics devices and technologies for data storage and computation [1–3]. Current-induced magnetization switching is presently used in magnetic random-access memory through spin-transfer torque [4,5]. However, the inclusion of electric current inevitably involves Joule heating and therefore high-energy dissipation. An important objective is therefore to identify a way to electrically switch the directions of spins with very low dissipation. In spintronics, major efforts have been devoted to optimizing the choice of materials and hybrid structures [6–10] in order to reduce the power consumption for switching, making it comparable to that in present semiconductor field-effect transistors [11].

At low temperatures, an obvious candidate for achieving low-dissipation electric control over magnetism is superconducting materials due to their ability to host dissipationless supercurrents. Combining superconductivity and spintronics [12] offers possibilities to achieve supercurrent-induced magnetization dynamics, by which Joule heating and dissipation can be minimized. To achieve this, several theory papers have proposed to utilize spin-polarized triplet supercurrents [13], which have been experimentenlly verified in superconductor (SC)/ferromagnet (FM) Josephson junctions [14–17]. It has also been theoretically shown that triplet supercurrents can induce spin-transfer torque switching [18–20] and magnetization dynamics [21–27]. However, there exists no experimental observation of supercurrent-induced torque or magnetization dynamics. Part of the challenge lies within the complexity of the appropriate fabrication of the SC/FM multilayered structures, in which the SC/FM interface plays an essential role to create the triplet Cooper pairs for spin-polarized supercurrent.

In this work, we theoretically demonstrate a new and conceptually simple way in which the goal of spin switching via singlet supercurrents can be achieved. We consider a conventional SC and two spin impurities placed on its surface (see Fig. 1). Without the requirement of triplet Cooper pair or exotic material choices, this is a drastically simpler setup than previous studies, theoretical and experimental, that have considered magnetization dynamics in the superconducting state. By investigating the indirect exchange interaction between the two spin impurities, also known as the Ruderman-Kittel-Kasuya-Yosida (RKKY) interaction [28–30], we find that the spin orientation can be controlled by applying a supercurrent flowing through the SC. In the presence of the supercurrent, the quasiparticle bands become asymmetric in momentum space due to the broken parity symmetry, which also modulates the RKKY interaction. Further, the resulting sign change in the RKKY interaction causes the preferred spin orientation to be switched between parallel and antiparallel alignments, both by varying the magnitude of the supercurrent as well as its direction, providing two experimental routes to observe this effect.

II. THEORY

We consider a conventional Bardeen-Cooper-Schrieffer (BCS) [31] SC with two impurity spins on its surface. For the superconducting part of the Hamilton operator, the presence of a supercurrent can be modeled by allowing the order parameter to have a phase gradient. Thus, we may write in real space

$$H_{\mathrm{SC}} = \frac{\Delta_0}{2}\sum_{i\alpha\beta} e^{\mathrm{i}\boldsymbol{Q}\cdot\boldsymbol{r}_i}(\mathrm{i}\sigma^y)_{\alpha\beta}c^\dagger_{i\alpha}c^\dagger_{i\beta} + \mathrm{H.c.} \tag{1}$$

Here, Δ_0 is the magnitude of the superconducting order parameter, $\boldsymbol{Q}$ quantifies the magnitude and direction of the supercurrent, whereas $c^\dagger_{i\sigma}$ are electron creation operators at site i for spin σ. For $\boldsymbol{Q}=0$, H_{SC} reduces to the standard BCS Hamiltonian.

The full Hamilton operator for the superconducting part, which includes a hopping term, takes the form

$$H_0 = \frac{1}{2}\sum_{\boldsymbol{k}\sigma}\phi^\dagger_{\boldsymbol{k}\sigma}\begin{pmatrix}\varepsilon_{\boldsymbol{k}} & \sigma\Delta_0\\ \sigma\Delta_0 & -\varepsilon_{-\boldsymbol{k}-\boldsymbol{Q}}\end{pmatrix}\phi_{\boldsymbol{k}\sigma}, \tag{2}$$

after performing a Fourier transformation $c^\dagger_{i\sigma} = \frac{1}{\sqrt{N}}\sum_{\boldsymbol{k}} c^\dagger_{\boldsymbol{k}\sigma}e^{\mathrm{i}\boldsymbol{k}\cdot\boldsymbol{r}_i}$ where N is the total number of the lattice points. Above, $\varepsilon_{\boldsymbol{k}} = -2t[\cos(k_x a)+\cos(k_z a)]-\mu$ is the dispersion relation, in which t is the hopping parameter, a is the lattice constant, and μ is the chemical potential. Here a 2D model in the xz plane is chosen for concreteness and $\phi_{k\sigma}^{\dagger} = (c_{k\sigma}^{\dagger} \quad c_{-k-Q,-\sigma})$ is the fermion basis. The two pairs of energy eigenvalues and eigenstates of the matrix in Eq. (2) are obtained as E_k^+ with $(u_k, \sigma v_k)^T$ and E_k^- with $(-\sigma v_k, u_k)^T$, in which

$$E_k^{\pm} = \tfrac{1}{2}\left(\varepsilon_k - \varepsilon_{-k-Q} \pm \sqrt{(\varepsilon_k + \varepsilon_{-k-Q})^2 + 4\Delta_0^2}\right) \tag{3}$$

and

$$u_k(v_k) = \sqrt{\frac{1}{2}\left(1 + (-)\frac{\varepsilon_k + \varepsilon_{-k-Q}}{\sqrt{(\varepsilon_k + \varepsilon_{-k-Q})^2 + 4\Delta_0^2}}\right)}. \tag{4}$$

Based on the eigenpairs, the Hamiltonian is diagonalized as

$$H_0 = \frac{1}{2}\sum_{k\sigma}(E_k^+ - E_{-k-Q}^-)\gamma_{k\sigma}^{\dagger}\gamma_{k\sigma}, \tag{5}$$

where the operators satisfy

$$\phi_{k\sigma} = \begin{pmatrix} c_{k\sigma} \\ c_{-k-Q,-\sigma}^{\dagger} \end{pmatrix} = \begin{pmatrix} u_k & -\sigma v_k \\ \sigma v_k & u_k \end{pmatrix}\begin{pmatrix} \gamma_{k\sigma} \\ \gamma_{-k-Q,-\sigma}^{\dagger} \end{pmatrix}. \tag{6}$$

To model the impurity spins interacting with the SC, we consider a Hamilton operator which is treated as a perturbation:

$$\Delta H = J\sum_j \boldsymbol{S}_j \cdot \boldsymbol{s}_j, \tag{7}$$

in which J is the strength of the interaction between the impurity classical spin $\boldsymbol{S}_j$ and the conduction electron spin $\boldsymbol{s}_j = \sum_{\alpha\beta} c_{j\alpha}^{\dagger}\boldsymbol{\sigma}_{\alpha\beta}c_{j\beta}$ where $\boldsymbol{\sigma}$ denotes the Pauli matrix vector. We set $S \equiv |\boldsymbol{S}_j| = 1$, meaning that the magnitude of the impurity spin is absorbed into the coupling constant J.

After Fourier transforming and expressing the c operators in terms of γ operators described by Eq. (6), we obtain

$$\begin{aligned}\Delta H = \sum_{kk'\alpha\beta} T_{kk'\alpha\beta}[&u_k^* u_{k'}\gamma_{k\alpha}^{\dagger}\gamma_{k'\beta} - \beta u_k^* v_{k'}\gamma_{k\alpha}^{\dagger}\gamma_{-k'-Q,-\beta}^{\dagger} \\ &- \alpha v_k^* u_{k'}\gamma_{-k-Q,-\alpha}\gamma_{k'\beta} + \alpha\beta v_k^* v_{k'}\gamma_{-k-Q,-\alpha}\gamma_{-k'-Q,-\beta}^{\dagger}],\end{aligned} \tag{8}$$

in which $T_{kk'\alpha\beta} = \sum_j \frac{J}{N}e^{i(k-k')\cdot r_j}\boldsymbol{S}_j\cdot\boldsymbol{\sigma}_{\alpha\beta}$ is defined.

We now perform a Schrieffer-Wolff transformation to obtain the RKKY interaction between the impurity spins, mediated by the SC. This is in essence a second-order perturbation theory for ΔH achieved by applying a canonical transformation $H_{\text{eff}} = e^{\eta S}He^{-\eta S}$ for $H = H_0 + \Delta H$. Subsequently, one identifies ηS so that it satisfies $\Delta H + [\eta S, H_0] = 0$ which projects out the first-order effect of the perturbation, which does not generate any interaction between the impurity spins. This gives rise to the effective Hamiltonian

$$H_{\text{eff}} = H_0 + \tfrac{1}{2}[\eta S, \Delta H], \tag{9}$$

in which one can express ηS with the same operators as in Eq. (8): $\eta S = \sum_{kk'\alpha\beta}[A_{kk'\alpha\beta}\gamma_{k\alpha}^{\dagger}\gamma_{k'\beta} + B_{kk'\alpha\beta}\gamma_{k\alpha}^{\dagger}\gamma_{-k'-Q,-\beta}^{\dagger} + C_{kk'\alpha\beta}\gamma_{-k-Q,-\alpha}\gamma_{k'\beta} + D_{kk'\alpha\beta}\gamma_{-k-Q,-\alpha}\gamma_{-k'-Q,-\beta}^{\dagger}]$. The coefficients are consequently identified as

$$\begin{aligned}A_{kk'\alpha\beta} &= -\frac{2u_k^* u_{k'}T_{kk'\alpha\beta}}{E_{k'\beta}^+ - E_{-k'-Q,-\beta}^- - E_{k\alpha}^+ + E_{-k-Q,-\alpha}^-}, \\ B_{kk'\alpha\beta} &= -\frac{2\beta u_k^* v_{k'}T_{kk'\alpha\beta}}{E_{k\alpha}^+ - E_{-k-Q,-\alpha}^- + E_{-k'-Q,-\beta}^+ - E_{k'\beta}^-}, \\ C_{kk'\alpha\beta} &= \frac{2\alpha v_k^* u_{k'}T_{kk'\alpha\beta}}{E_{k'\beta}^+ - E_{-k'-Q,-\beta}^- + E_{-k-Q,-\alpha}^+ - E_{k\alpha}^-}, \\ D_{kk'\alpha\beta} &= \frac{2\alpha\beta v_k^* v_{k'}T_{kk'\alpha\beta}}{E_{-k'-Q,-\beta}^+ - E_{k'\beta}^- - E_{-k-Q,-\alpha}^+ + E_{k\alpha}^-}.\end{aligned} \tag{10}$$

Given ηS, the expectation value of the effective Hamiltonian given by Eq. (9) may now be evaluated to obtain the RKKY interaction.

III. RESULTS AND DISCUSSION

Defining $S_j^{\alpha\beta} \equiv \boldsymbol{S}_j\cdot\boldsymbol{\sigma}_{\alpha\beta}$ and using $\Sigma_{\alpha\beta}S_j^{\alpha\beta}S_i^{\beta\alpha} = 2\boldsymbol{S}_i\cdot\boldsymbol{S}_j$ and $\Sigma_{\alpha\beta}\alpha\beta S_j^{\alpha\beta}S_i^{-\alpha,-\beta} = -2\boldsymbol{S}_i\cdot\boldsymbol{S}_j$, we obtain the expectation value

$$\langle H_{\text{eff}}\rangle = E_0 + \Sigma_{ij}E_{\text{RKKY}}\boldsymbol{S}_i\cdot\boldsymbol{S}_j, \tag{11}$$

in which E_0 is a constant and E_{RKKY} describes the RKKY interaction. The sum $\sum_{ij}$ in Eq. (11) is over the two impurity spins. Applying $u_k = u_{-k-Q}$, $v_k = v_{-k-Q}$ and $E_k^{\pm} = -E_{-k-Q}^{\mp}$, the RKKY interaction can after lengthy calculations be expressed via the quantities

$$\begin{aligned}F_1(\boldsymbol{k},\boldsymbol{k}') &= (|u_k u_{k'}|^2 + u_k^* u_{k'} v_k^* v_{k'})\frac{n(E_k^+) - n(E_{k'}^+)}{E_{k'}^+ - E_k^+}, \\ F_2(\boldsymbol{k},\boldsymbol{k}') &= (-|u_k v_{k'}|^2 + u_k^* u_{k'} v_k^* v_{k'})\frac{n(E_k^+) + n(E_{-k'-Q}^+) - 1}{E_k^+ + E_{-k'-Q}^+}, \\ F_3(\boldsymbol{k},\boldsymbol{k}') &= (u_k^* u_{k'} v_k^* v_{k'} - |u_{k'} v_k|^2)\frac{n(E_{k'}^+) + n(E_{-k-Q}^+) - 1}{E_{k'}^+ + E_{-k-Q}^+}, \\ F_4(\boldsymbol{k},\boldsymbol{k}') &= (u_k^* u_{k'} v_k^* v_{k'} + |v_k v_{k'}|^2)\frac{n(E_{-k-Q}^+) - n(E_{-k'-Q}^+)}{E_{-k'-Q}^+ - E_{-k-Q}^+},\end{aligned} \tag{12}$$

in the following form

$$\begin{aligned}E_{\text{RKKY}} = -\left(\frac{J}{N}\right)^2 \Sigma_{kk'}e^{i(k-k')\cdot R_{ij}}[&F_1(\boldsymbol{k},\boldsymbol{k}') + F_2(\boldsymbol{k},\boldsymbol{k}') \\ &+ F_3(\boldsymbol{k},\boldsymbol{k}') + F_4(\boldsymbol{k},\boldsymbol{k}')],\end{aligned} \tag{13}$$

where $\boldsymbol{R}_{ij} = \boldsymbol{r}_j - \boldsymbol{r}_i$ and $n(E) = (1 + e^{\beta E})^{-1}$ denotes the Fermi-Dirac distribution at energy E with $\beta = 1/k_BT$. The above expression can be further simplified since E_{RKKY} is real, and thus the exponential prefactor can be replaced with its corresponding cosine component. Subsequently, one observes that the contribution from F_2 is the same as F_3, which can be seen by renaming indices $\boldsymbol{k} \leftrightarrow \boldsymbol{k}'$ and using that u, v are real.

For $\boldsymbol{Q} = 0$, we regain the results studied previously in the literature for RKKY interaction in SCs [32–35] in the form

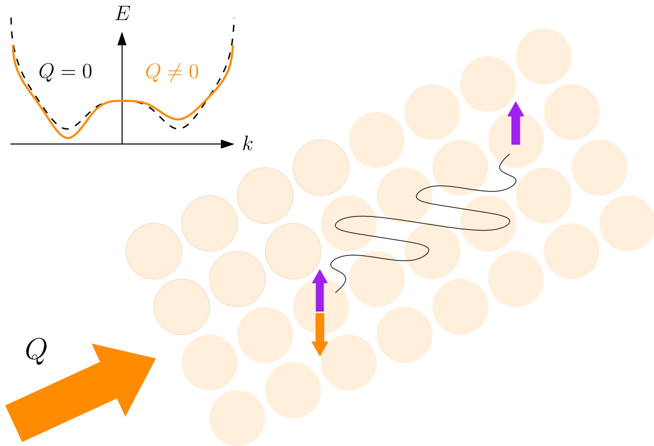

FIG. 1. Two impurity spins (purple small arrows) are coupled via the RKKY interaction (wavy black line) mediated by conduction band quasiparticles in the superconducting state. The picture shows a scenario where a parallel spin orientation is energetically preferred. When a supercurrent (large orange arrow) is applied, giving the Cooper pairs a finite momentum Q, the quasiparticle bands become asymmetric in momentum k (upper part of the plot), due to the broken parity symmetry. This causes a change in the RKKY interaction which can now favor the opposite spin orientation, in this case antiparallel (small orange arrow). In this way, the supercurrent induces spin switching.

of an additional antiferromagnetic, exponentially decaying term that appears in E_{RKKY} along with the usual rapidly oscillating interaction. Equation (13) can then be numerically evaluated to determine the effect of a supercurrent on the spin-spin interaction. To estimate a reasonable magnitude for the momentum $Q = |\boldsymbol{Q}|$ of the Cooper pairs, we note that the critical supercurrent that a SC can sustain is provided by $Q\xi \simeq 1$ [36] where $\xi = \hbar v_F/(\pi \Delta_0)$ is the coherence length. An analytical estimate for Q can be given for a simple one-dimensional (1D) model. The Fermi velocity in our lattice model is defined via $v_F = \frac{1}{\hbar}(d\varepsilon_k/dk)|_{k=k_F}$ where k_F is obtained as the momentum where $\varepsilon_k = 0$. To maximize the value of Q (in order to have a supercurrent which can strongly influence the RKKY interaction), one ideally needs a SC with as small ξ as possible. High-T_c superconductors can have $\xi \simeq 3a$, allowing $Q \simeq 0.3/a$. Subsequently, μ and Δ_0 should be chosen to get $\xi \simeq 3a$. Choosing $\mu = -1.8t$, one finds from $-2t\cos(ka) - \mu = 0$ that $k_F \simeq 0.5/a$, which gives $v_F \simeq at/\hbar$. Then, for $\Delta_0/t = 0.1$, we can achieve $\xi \simeq 3a$ which gives the upper limit $Q \simeq 0.3/a$. Similar parameters were used in Ref. [37]. To use a more realistic value for Δ, the system size L would have to increase dramatically to ensure $L > \xi$ since $\xi \propto \Delta^{-1}$, making the computational demands unfeasible. This is a known computational challenge with the lattice Bogoliubov–de Gennes framework, which nevertheless is known to produce predictions that compare well qualitatively, and in some cases even quantitatively, with experiments [38].

The RKKY interaction results are shown in Fig. 2 for $Q = 0.1/a$. We show results both for zero supercurrent ($Q = 0$), and supercurrent flowing parallell ($\parallel$) and perpendicular ($\perp$) to the separation vector $\boldsymbol{R}_{ij}$ of the two spin impurities. Here we fix $\boldsymbol{Q}$ along $\boldsymbol{x}$ and consider $\boldsymbol{R}_{ij}$ along $\boldsymbol{x}$ (z) to cover the $\parallel$ ($\perp$) configuration. The figure demonstrates that the RKKY interaction changes its sign within several separation-distance regimes by tuning the magnitude and direction of the supercurrent. Since $E_{\text{RKKY}} < 0$ causes a parallel (P) alignment of the two spin impurities while $E_{\text{RKKY}} > 0$ supports an antiparallel (AP) orientation, the sign change thus induces spin switching between the P and AP states. In addition, the RKKY curves are almost the same for the $Q = 0$ and $\perp$ cases. This can be explained by the energy dispersion symmetry breaking induced by the supercurrent, which is the strongest for the quasiparticles mediating the RKKY interaction when $\boldsymbol{Q} \parallel \boldsymbol{R}_{ij}$ and negligible for the perpendicular case when Q is small. In Fig. 2, the black arrows denote spin switching achieved by changing the direction of supercurrent flow (between $\boldsymbol{Q} \parallel \boldsymbol{R}_{ij}$ and $\boldsymbol{Q} \perp \boldsymbol{R}_{ij}$). The black arrows also indicate switching caused by turning the supercurrent on and off (between $\boldsymbol{Q} \parallel \boldsymbol{R}_{ij}$ and $\boldsymbol{Q} = 0$) since the $Q = 0$ and $\perp$ cases essentially coincide due to the small value of Q. It is clear from the arrows in the figure that the presence of supercurrent gives rise to ample opportunities for spin switching at several separation distances. Note that for each arrow, the switch occurs in a finite interval centered around the position of the arrow and not just exactly at the location of the arrow, making the switching effect more accessible.

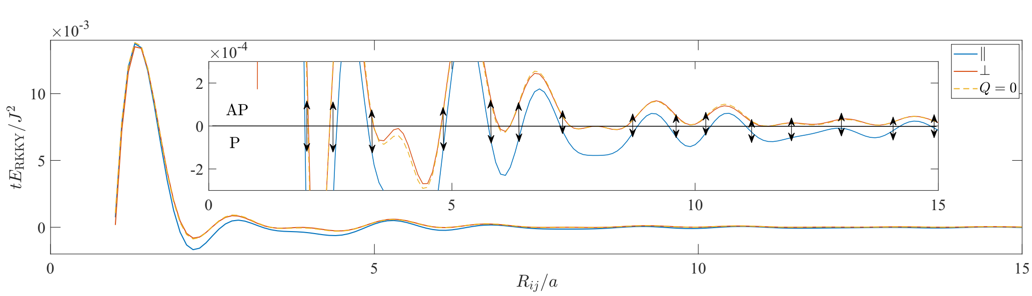

FIG. 2. Normalized RKKY interaction between two impurity spins on top of a current-carrying superconductor with $Qa = 0.1$. The inset shows a zoom-in of the main plot and the horizontal black line is a guide to the eye for where the RKKY interaction changes from P to AP. The direction of the supercurrent is along the impurity separation distance for $\parallel$ and perpendicular to it for $\perp$. $E_{\text{RKKY}} > 0$ favors an AP alignment of the spins, whereas $E_{\text{RKKY}} < 0$ favors a P alignment. The arrows show the preferred spin alignment is altered by either turning the supercurrent on and off or by changing its direction between $\parallel$ and $\perp$. Since the supercurrent magnitude is small for $Qa = 0.1$, the $Q = 0$ and $\perp$ cases essentially coincide. We consider $\mu/t = -1.8$, $\Delta_0/t = 0.1$, $k_BT/t = 0.01$, $Q = 0.1/a$, and $N = 10^4$ sites.

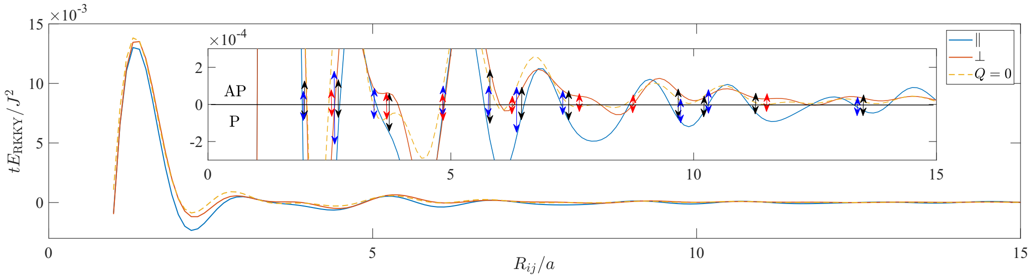

FIG. 3. Same as in Fig. 2, but for $Qa = 0.2$. Since the supercurrent is now larger than in Fig. 2, additional spin switching is enabled. Namely, the preferred spin alignment is switched by either turning the supercurrent on and off in the $\parallel$ direction (blue arrows), on and off in the $\perp$ direction (red arrows), or changing the direction of the supercurrent between $\parallel$ and $\perp$ (black arrows). We consider $\mu/t = -1.8$, $\Delta_0/t = 0.1$, $k_BT/t = 0.01$, $Q = 0.2/a$, and $N = 10^4$ sites.

We also show results in Fig. 3 for a slightly larger value of the supercurrent, $Q = 0.2/a$, demonstrating the robustness of the effect and that there exists an abundance of possible switching effects by either turning of the supercurrent or by changing its direction. As Q increases, compared with $Q = 0.1/a$ in Fig. 2, the difference between the $Q = 0$ and $\perp$ cases becomes distinguishable and the additional spin switching between them becomes possible, as the red arrows show.

Finally, we plot the RKKY interaction energy at a fixed lattice site as a function of the supercurrent magnitude Q in Fig. 4 for two site choices. The supercurrent flow starts modifying E_{RKKY} at much smaller values of Q when it flows along $\boldsymbol{R}_{ij}$ compared to when it flows perpendicular to it. The physical mechanism behind this is the directional dependence of the asymmetry in the quasiparticle bands $E_{\boldsymbol{k}}$ created by $\boldsymbol{Q}$. As mentioned before, the asymmetry is strongest for particles moving between the impurity spins when $\boldsymbol{Q} \parallel \boldsymbol{R}_{ij}$, which are precisely the ones contributing the most to the RKKY interaction. The lower panel of Fig. 4 shows that at a fixed separation distance $R_{ij} = |\boldsymbol{R}_{ij}|$, modulating the supercurrent magnitude Q can cause the preferred spin orientation to switch between P ($E_{\mathrm{RKKY}} < 0$) and AP ($E_{\mathrm{RKKY}} > 0$), which is consistent with the switching results observed in Figs. 2 and 3. The supercurrent-induced switching predicted here is most clear in the regime $T \ll T_c$. Thermal broadening reduces the difference between $\boldsymbol{Q} \parallel \boldsymbol{R}_{ij}$ and $\boldsymbol{Q} \perp \boldsymbol{R}_{ij}$ due to a strong suppression of the gap as $T \simeq T_c$, but becoming noticeable also from $T/T_c \simeq 0.5$ due to an increase in thermal excitations of quasiparticles.

An approximative analytical expression for the RKKY interaction with supercurrent can be derived under simplifying assumptions. For impurity separation distances $R \ll \xi$, one finds in 1D:

$$E_{\mathrm{RKKY}} = E_0(R) + 4\pi^3 J^2 \cos^2(k_F R) \int_0^\infty d\Omega \times \frac{\Delta^2\Omega^2\tilde{Q}^2}{(\Omega^2+\Delta^2)^3} e^{-\frac{2\Omega R}{\hbar v_F}}, \tag{14}$$

where $E_0(R)$ is the RKKY interaction for two impurity spins in a superconductor without supercurrent and $\tilde{Q} = \hbar v_F Q/2$ (see Appendix for details). As is physically reasonable, the lowest-order supercurrent-induced correction is quadratic in Q since the interaction should not distinguish between left- and right-going supercurrents. We also note that upon increasing T, Δ is suppressed and the RKKY interaction reverts back to its normal-state behavior where it is damped like R^{-2} in 2D.

We also give an estimate for the effect of the supercurrent Oersted field acting on the impurity spins via a Zeeman effect, and show that it is negligible compared to the RKKY interaction. Considering a thin superconducting film of thickness d with a critical current density $J_c = 10^7$ A/cm^2, the field at the surface can be approximated as $B = \mu_0 J_c d/2$ at the critical supercurrent strength. For $d = 15$ nm, this gives $B \simeq 10^{-3}$ T, corresponding to a very small Zeeman coupling $E_Z \simeq 10^{-5}$ meV at about half of the critical current density.

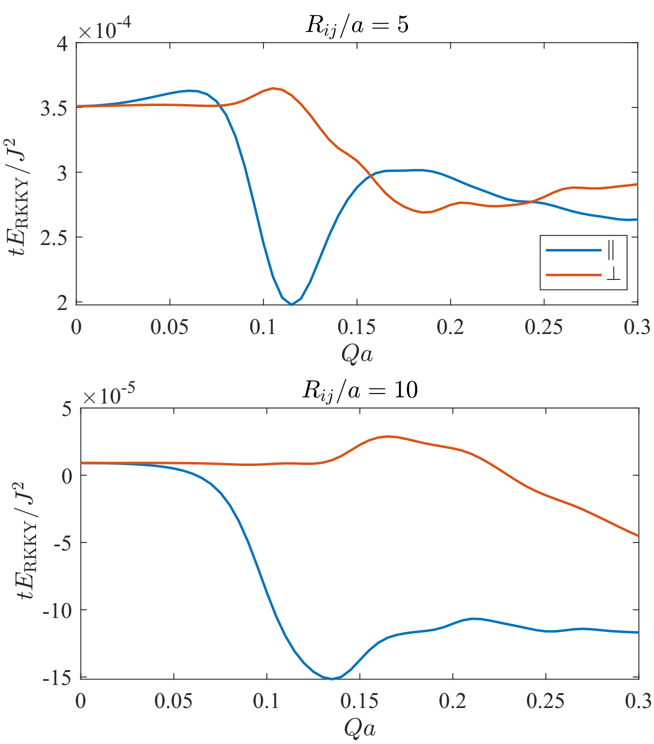

FIG. 4. Normalized RKKY interaction as a function of supercurrent magnitude. We consider two separation distances in the top and bottom panels and consider both a supercurrent flow along ($\parallel$) the separation distance vector and perpendicular ($\perp$) to it. We set $\mu/t = -1.8$, $\Delta_0/t = 0.1$, $k_BT/t = 0.01$, and $N = 10^4$ sites.

This can be compared to tE_{RKKY}/J^2 in our plots, which is typically of order 10^{-4} at a separation distance of several lattice sites. Using a weak-impurity spin coupling $J = 0.05t < \Delta_0$, as appropriate for the perturbative approach employed here, we get for $t = 500\,\mathrm{meV}$ that $E_{\mathrm{RKKY}} \simeq 10^{-4}\,\mathrm{meV}$ which is $\gg E_Z$. Although this is a rough estimate, we note that larger couplings J, outside the regime of our approach, between the impurity and conduction electron spins are accessible experimentally [39]. This will make the RKKY interaction even larger, in particular compared to the Oersted-field effect. A thinner SC film decreases the Oersted field further. The effect of supercurrent flow in the strong-coupling regime could be an interesting topic for future studies where in-gap Yu-Shiba-Rusinov (YSR) states [40–42] are expected to have a more prominent role. Quantitatively, the weak- and strong-coupling regimes are distinguished by the direct interaction strength J being substantially smaller or greater than the superconducting gap Δ_0, respectively. The main conclusion of this work, being the tunability of the RKKY interaction and thus the possibility to switch the ground-state spin configuration, is expected to hold also in this case. We also note that our work is distinct from previous literature considering a microwave-induced spin-spin interaction in the presence of YSR states [43] and magnetic instabilities induced in correlated normal metals induced by a supercurrent [37].

We also comment on the effect of nonmagnetic impurity scattering which will influence two aspects of the system. One is that it could influence the magnitude of the superconducting gap and critical temperature, if solved self-consistently. However, since we consider BCS s-wave superconductors, we expect that impurities have very little influence on the superconducting transition even for impurity magnitudes ranging up toward t [44]. Secondly, the presence of impurities is known to cause the RKKY interaction to decay more rapidly with distance if one averages over different impurity configurations [45]. For a fixed impurity configuration, however, it only introduces a phase shift in the distance dependence of the RKKY-interaction function. A similar effect could also be present in the superconducting state considered here. It is possible to add the nonmagnetic impurity scattering in the Bogoliubov–de Gennes formalism by considering a finite-size system where impurities are modeled as an on-site potential on randomly chosen sites. We leave this investigation for future work.

IV. CONCLUDING REMARKS

Our proposed system setup should be experimentally feasible. In Ref. [46], the RKKY interaction between Cr impurity spins coupled to a SC was studied using scanning-tunneling spectroscopy. All that is required in addition to observe the supercurrent-induced spin switching is the application of a current bias to the SC. We hope that the present work will stimulate the anticipated experimental realization of supercurrent-induced spin switching.

ACKNOWLEDGMENTS

M. Amundsen, J. A. Ouassou, and T. Yokoyama are thanked for helpful discussions. This work was supported by the Research Council of Norway through Grant No. 323766 and its Centres of Excellence funding scheme Grant No. 262633 “QuSpin.” Support from Sigma2—the National Infrastructure for High-Performance Computing and Data Storage in Norway, Project No. NN9577K, is acknowledged.

APPENDIX A: MATSUBARA GREEN FUNCTIONS

Here we present the derivation details of the analytical expression of the RKKY interaction in a 1D s-wave superconductor (SC) with supercurrent $\boldsymbol{Q}$ based on Matsubara Green functions for interested readers, in which $\boldsymbol{Q}$ has to be treated perturbatively in order to permit an analytical solution. The case with a larger $\boldsymbol{Q}$ which enables spin switching is shown numerically in the main text.

The s-wave SC with supercurrent $\boldsymbol{Q}$ can be described by the Hamiltonian

$$\hat{H} = \begin{pmatrix} \xi_+ & \Delta \\ \Delta & -\xi_- \end{pmatrix}, \tag{A1}$$

in which $\xi_\pm = \xi_{\boldsymbol{k}\pm\boldsymbol{Q}/2}$. Note this Hamiltonian is equivalent to that described by Eq. (2) in the main text by a mere relabeling of momentum index. The momentum-dependent Matsubara Green function can be obtained as

$$\begin{aligned}\hat{G}^M &= (i\Omega - \hat{H})^{-1} \\ &= -\frac{1}{\Omega^2 + i\Omega(\xi_+ - \xi_-) + \xi_+\xi_- + \Delta^2} \\ &\quad\times \begin{pmatrix} i\Omega + \xi_- & \Delta \\ \Delta & -\xi_+ + i\Omega \end{pmatrix},\end{aligned} \tag{A2}$$

in which Ω is the fermionic Matsubara frequency. Therefore, we have the (11)/(12) matrix element as the normal/anomalous Green function:

$$G^M(i\Omega, \boldsymbol{k}, \boldsymbol{Q}) = -\frac{i\Omega + \xi_-}{\Omega^2 + i\Omega(\xi_+ - \xi_-) + \xi_+\xi_- + \Delta^2}, \tag{A3}$$

$$F^M(i\Omega, \boldsymbol{k}, \boldsymbol{Q}) = -\frac{\Delta}{\Omega^2 + i\Omega(\xi_+ - \xi_-) + \xi_+\xi_- + \Delta^2}. \tag{A4}$$

Substitute the approximation that $\xi_\pm = \xi_{\boldsymbol{k}} \pm \hbar\boldsymbol{v}_F\boldsymbol{Q}/2$ [47], the normal and anomalous Green functions can be simplified as

$$G^M(i\Omega, \boldsymbol{k}, \boldsymbol{Q}) = -\frac{i\Omega + \xi_{\boldsymbol{k}} - \hbar\boldsymbol{v}_F\boldsymbol{Q}/2}{(\Omega + i\hbar\boldsymbol{v}_F\boldsymbol{Q}/2)^2 + \xi_{\boldsymbol{k}}^2 + \Delta^2}, \tag{A5}$$

$$F^M(i\Omega, \boldsymbol{k}, \boldsymbol{Q}) = -\frac{\Delta}{(\Omega + i\hbar\boldsymbol{v}_F\boldsymbol{Q}/2)^2 + \xi_{\boldsymbol{k}}^2 + \Delta^2}, \tag{A6}$$

in which $\boldsymbol{v}_F$ is the Fermi velocity.

Consider 1D SC, use the standard approximation of linearizing the dispersion close to the Fermi level

$$\xi_k = \left(p^2 - p_F^2\right)/2m \approx \hbar v_F(k \times \mathrm{sign}(\mathrm{Re}\{k\}) - k_F), \tag{A7}$$

where k_F is the Fermi wave vector, and we have the Fourier-transformed normal Matsubara Green function

$$\begin{aligned}G^M(i\Omega,\pm R,Q) &= \int_{-\infty}^{+\infty}\frac{dk}{2\pi}G(i\Omega,k,Q)e^{\pm ikR}\\ &= -\int_{-\infty}^{\infty}\frac{dk}{(2\pi)}\frac{i\Omega+\hbar v_F[k\times \mathrm{sign}(\mathrm{Re}\{k\})-k_F-Q/2]}{(\Omega+i\hbar v_F Q/2)^2+\Delta^2+[\hbar v_F(k\times \mathrm{sign}(\mathrm{Re}\{k\})-k_F)]^2}\mathrm{e}^{\pm ikR}\\ &= -\frac{1}{2\pi\hbar^2 v_F^2}\int_{-\infty}^{+\infty}dk\frac{i\Omega+\hbar v_F[k\times \mathrm{sign}(\mathrm{Re}\{k\})-k_F-Q/2]}{\left(k\times \mathrm{sign}(\mathrm{Re}\{k\})-k_F+i\frac{\sqrt{(\Omega+i\hbar v_F Q/2)^2+\Delta^2}}{\hbar v_F}\right)\left(k\times \mathrm{sign}(\mathrm{Re}\{k\})-k_F-i\frac{\sqrt{(\Omega+i\hbar v_F Q/2)^2+\Delta^2}}{\hbar v_F}\right)}e^{\pm ikR}.\end{aligned} \tag{A8}$$

This integrand has simple poles at

$$k=\pm k_F\pm' i\sqrt{(\Omega+i\hbar v_F Q/2)^2+\Delta^2}/(\hbar v_F), \tag{A9}$$

where $\hbar v_F Q/2<\Delta$ is considered to make further analytical progress (also ensuring that the supercurrent remains below its critical value). A similar procedure can be applied to obtain the Fourier-transformed anomalous Matsubara Green function.

To compute $G^M(i\Omega,R,Q)$ and $F^M(i\Omega,R,Q)$, we consider the upper half-plane which includes two poles at $\pm k_F+i\frac{\sqrt{(\Omega+i\hbar v_F Q/2)^2+\Delta^2}}{\hbar v_F}$ and use the residue theorem as $G^M(i\Omega,R,Q)=2\pi i[\mathrm{Res}\{\mathrm{pole1}\}+\mathrm{Res}\{\mathrm{pole2}\}]$:

$$G^M(i\Omega,R,Q)=-\frac{i}{\hbar v_F}\left[\frac{\Omega+i\hbar v_F Q/2}{\sqrt{(\Omega+i\hbar v_F Q/2)^2+\Delta^2}}\cos(k_F R)+i\sin(k_F R)\right]e^{-\frac{\sqrt{(\Omega+i\hbar v_F Q/2)^2+\Delta^2}}{\hbar v_F}R}, \tag{A10}$$

$$F^M(i\Omega,R,Q)=-\frac{1}{\hbar v_F}\frac{\Delta}{\sqrt{(\Omega+i\hbar v_F Q/2)^2+\Delta^2}}\cos(k_F R)e^{-\frac{\sqrt{(\Omega+i\hbar v_F Q/2)^2+\Delta^2}}{\hbar v_F}R}. \tag{A11}$$

To compute $G^M(i\Omega,-R,Q)$ and $F^M(i\Omega,-R,Q)$, we consider the lower half-plane which includes two poles at $\pm k_F-i\frac{\sqrt{(\Omega+i\hbar v_F Q/2)^2+\Delta^2}}{\hbar v_F}$ and use $G^M(i\Omega,-R,Q)=-2\pi i[\mathrm{Res}\{\mathrm{pole1}\}+\mathrm{Res}\{\mathrm{pole2}\}]$. It is found that $G^M(i\Omega,R,Q)=G^M(i\Omega,-R,Q)$ and $F^M(i\Omega,R,Q)=F^M(i\Omega,-R,Q)$.

APPENDIX B: DERIVATION OF THE RKKY EXPRESSION

As derived in Ref. [48] [see Eq. (C8)], the RKKY interaction in terms of the retarded Green function is given by

$$\begin{aligned}E_{\mathrm{RKKY}} &= 2\pi^3J^2\mathrm{Im}\int_{-\infty}^{+\infty}d\omega\tanh\left(\frac{\omega}{2T}\right)\\ &\times\left[G_\omega^R(R)G_\omega^R(-R)+F_\omega^R(R)\tilde{F}_\omega^R(-R)\right].\end{aligned} \tag{B1}$$

In what follows, we omit the constant prefactor $2\pi^3J^2$, where J is the exchange-coupling strength, for brevity of notation. $G_\omega^R(R)$ and $F_\omega^R(R)$ are the normal and anomalous retarded Green functions in the real space, respectively. In the momentum space, we have $\tilde{F}_\omega^R(-R)=\frac{1}{2\pi}\int dk\tilde{F}_\omega^R(k)e^{-ikR}$ and $\tilde{F}_\omega^R(k)=[F_{-\omega}^R(-k)]^*$. Here, ω is real energy. Note that $\tanh(\omega/2T)=1-2n_F(\omega)$ where n_F is Fermi-Dirac distribution. The contribution from the resulting 1-term in the integral vanishes if the poles of the retarded Green function lie in the complex lower half-plane. (The vanishing integral is obtained by closing the contour in the upper half-plane). That the poles of the retarded Green function conventionally lie in the lower complex half-plane is seen as follows. First, write $G_\omega^R(R)$ as $\int dk\mathrm{e}^{ikR}G_\omega^R(k)$. Then, we have to determine where the poles of $G_\omega^R(k)$ lie in the complex ω plane. In general, the retarded Green function can have a self-energy Σ, and the imaginary part of this must be negative in order to interpret $-\mathrm{Im}\,\Sigma$ as the inverse lifetime of the quasiparticle. $F_\omega^R(k)$ shares the same denominator and therefore same poles as $G_\omega^R(k)$. Using this, we obtain the expression

$$\begin{aligned}E_{\mathrm{RKKY}} &= -2\mathrm{Im}\int_{-\infty}^{+\infty}d\omega\, n_F(\omega)\\ &\times\left[G_\omega^R(R)G_\omega^R(-R)+F_\omega^R(R)\tilde{F}_\omega^R(-R)\right].\end{aligned} \tag{B2}$$

At zero temperature, this reduces to

$$E_{\mathrm{RKKY}}=-2\mathrm{Im}\int_{-\infty}^{0}d\omega\left[G_\omega^R(R)G_\omega^R(-R)+F_\omega^R(R)\tilde{F}_\omega^R(-R)\right]. \tag{B3}$$

Next, we convert this expression to be in terms of Matsubara Green functions. It is known that

$$G_\omega^R=G^M(\omega+i\delta),\quad F_\omega^R=F^M(\omega+i\delta), \tag{B4}$$

where δ is a positive infinitesimal. This general relation is easily verified for a normal metal where

$$\begin{aligned}G_\omega^R &= \frac{1}{\omega-\xi_k+i\delta},\\ G^M(i\Omega) &= \frac{1}{i\Omega-\xi_k}.\end{aligned} \tag{B5}$$

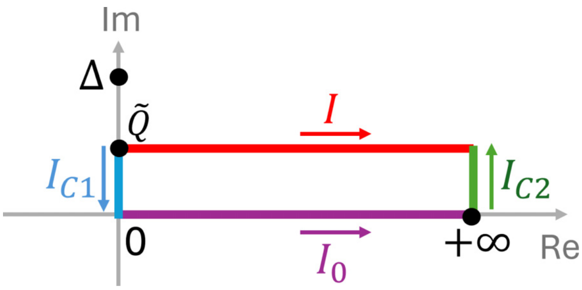

FIG. 5. Integral contour to calculate I_{1-3}.

Here for a 1D SC with supercurrent Q, we need to be careful with $\tilde{F}^R$:

$$F^R_\omega(k,Q) = \frac{\Delta}{(\omega + i\delta - \hbar v_F Q/2)^2 - \xi_k^2 - \Delta^2}, \tag{B6}$$

$$\begin{aligned}\tilde{F}^R_\omega(k,Q) &= \left[F^R_{-\omega}(-k,Q)\right]^* \\ &= \frac{\Delta}{(\omega + i\delta + \hbar v_F Q/2)^2 - \xi_k^2 - \Delta^2} \\ &= F^R_\omega(k,-Q),\end{aligned} \tag{B7}$$

$$\begin{aligned}\tilde{F}^R_\omega(-R,Q) &= \frac{1}{2\pi}\int dk \tilde{F}^R_\omega(k,Q)e^{-ikR} \\ &= \frac{1}{2\pi}\int dk F^R_\omega(k,-Q)e^{-ikR} \\ &= F^R_\omega(-R,-Q),\end{aligned} \tag{B8}$$

in which $\xi_k = \xi_{-k}$ is applied. We then rewrite

$$\begin{aligned}E_{\mathrm{RKKY}} = -2\mathrm{Im}\int_{-\infty}^{0} d\omega \big[&G^R_\omega(R,Q)G^R_\omega(-R,Q) \\ &+ F^R_\omega(R,Q)F^R_\omega(-R,-Q)\big].\end{aligned} \tag{B9}$$

Introducing the new variable Ω via $\omega = i\Omega - i\delta$ or $\Omega = -i\omega + \delta$, we get

$$\begin{aligned}E_{\mathrm{RKKY}} = -2\mathrm{Im}\int_{i\infty+\delta}^{\delta} id\Omega\, [&G^M(i\Omega,R,Q)G^M(i\Omega,-R,Q) \\ &+ F^M(i\Omega,R,Q)F^M(i\Omega,-R,-Q)].\end{aligned} \tag{B10}$$

Since $\mathrm{Im}(iz) = \mathrm{Re}(z)$, we obtain

$$\begin{aligned}E_{\mathrm{RKKY}} = -2\mathrm{Re}\int_{i\infty+\delta}^{\delta} d\Omega\, [&G^M(i\Omega,R,Q)G^M(i\Omega,-R,Q) \\ &+ F^M(i\Omega,R,Q)F^M(i\Omega,-R,-Q)].\end{aligned} \tag{B11}$$

The next step is to perform a Wick rotation, in which a quarter circle is drawn in the first quadrant of the complex plane. As long as there are no poles in the first quadrant, which lies in the upper complex Ω plane, we will have via the residue theorem that

$$\int_{i\infty+\delta}^{\delta} + \int_{\delta}^{\infty} = 0, \tag{B12}$$

since the arc contribution vanishes due to the Green functions vanishing sufficiently rapidly. Apply $\delta \to 0$, we finally arrive at

$$\begin{aligned}E_{\mathrm{RKKY}} = 2\mathrm{Re}\int_{0}^{\infty} d\Omega\, [&G^M(i\Omega,R,Q)G^M(i\Omega,-R,Q) \\ &+ F^M(i\Omega,R,Q)F^M(i\Omega,-R,-Q)].\end{aligned} \tag{B13}$$

APPENDIX C: ANALYTICAL INTEGRATION OF THE RKKY INTERACTION

Based on the previous expressions for Matsubara Green functions in Eqs. (A10)–(A11), we have

$$\begin{aligned}G^M(i\Omega,R,Q)G^M(i\Omega,-R,Q) = \frac{-1}{\hbar^2 v_F^2}&\left[\frac{(\Omega+i\tilde{Q})^2}{(\Omega+i\tilde{Q})^2+\Delta^2}\cos^2(k_F R) + \frac{\Omega+i\tilde{Q}}{\sqrt{(\Omega+i\tilde{Q})^2+\Delta^2}} i\sin(2k_F R) - \sin^2(k_F R)\right] \\ &\times e^{-\frac{2\sqrt{(\Omega+i\tilde{Q})^2+\Delta^2}}{\hbar v_F}R}\end{aligned} \tag{C1}$$

$$F^M(i\Omega,R,Q)F^M(i\Omega,-R,-Q) = \frac{1}{\hbar^2 v_F^2}\frac{\Delta^2}{\sqrt{[(\Omega+i\tilde{Q})^2+\Delta^2][(\Omega-i\tilde{Q})^2+\Delta^2]}}\cos^2(k_F R)e^{-\frac{\sqrt{(\Omega+i\tilde{Q})^2+\Delta^2}}{\hbar v_F}R-\frac{\sqrt{(\Omega-i\tilde{Q})^2+\Delta^2}}{\hbar v_F}R}, \tag{C2}$$

in which $\tilde{Q} = \hbar v_F Q/2$. Consider a superconducting correlation length $R_0 = \hbar v_F/\Delta$ much larger than the separation distance of the spins, meaning $R \ll R_0$ or $R/R_0 \to 0$ (i.e., $R\Delta/\hbar v_F \to 0$ in the exponents), the required integrals to calculate the RKKY interaction by Eq. (B13) are listed as follows:

$$I_1 = \mathrm{Re}\int_0^\infty d\Omega \frac{(\Omega+i\tilde{Q})^2}{(\Omega+i\tilde{Q})^2+\Delta^2}e^{-\frac{2\sqrt{(\Omega+i\tilde{Q})^2+\Delta^2}}{\hbar v_F}R} \approx \mathrm{Re}\int_0^\infty d\Omega \frac{(\Omega+i\tilde{Q})^2}{(\Omega+i\tilde{Q})^2+\Delta^2}e^{-\frac{2(\Omega+i\tilde{Q})}{\hbar v_F}R}, \tag{C3}$$

$$I_2 = \mathrm{Re}\int_0^\infty d\Omega \frac{\Omega+i\tilde{Q}}{\sqrt{(\Omega+i\tilde{Q})^2+\Delta^2}}ie^{-\frac{2\sqrt{(\Omega+i\tilde{Q})^2+\Delta^2}}{\hbar v_F}R} \approx \mathrm{Re}\int_0^\infty d\Omega \frac{\Omega+i\tilde{Q}}{\sqrt{(\Omega+i\tilde{Q})^2+\Delta^2}}ie^{-\frac{2(\Omega+i\tilde{Q})}{\hbar v_F}R}, \tag{C4}$$

$$I_3 = \mathrm{Re}\int_0^\infty d\Omega e^{-\frac{2\sqrt{(\Omega+i\tilde{Q})^2+\Delta^2}}{\hbar v_F}R} \approx \mathrm{Re}\int_0^\infty d\Omega e^{-\frac{2(\Omega+i\tilde{Q})}{\hbar v_F}R}, \tag{C5}$$

$$I_4 = \mathrm{Re}\int_0^\infty d\Omega \frac{\Delta^2}{\sqrt{[(\Omega+i\tilde{Q})^2+\Delta^2][(\Omega-i\tilde{Q})^2+\Delta^2]}} e^{-\frac{\sqrt{(\Omega+i\tilde{Q})^2+\Delta^2}}{\hbar v_F}R-\frac{\sqrt{(\Omega-i\tilde{Q})^2+\Delta^2}}{\hbar v_F}R}$$
$$\approx \mathrm{Re}\int_0^\infty d\Omega \frac{\Delta^2}{\sqrt{[(\Omega+i\tilde{Q})^2+\Delta^2][(\Omega-i\tilde{Q})^2+\Delta^2]}} e^{-\frac{2\Omega}{\hbar v_F}R}, \tag{C6}$$

in which the first three integrals come from Eq. (C1) and the last one comes from Eq. (C2).

For I_{1-3}, by changing variable $\Omega \to \Omega + i\tilde{Q}$, the three integrals become

$$I_1 = \mathrm{Re}\int_{i\tilde{Q}}^{\infty+i\tilde{Q}} d\Omega \frac{\Omega^2}{\Omega^2+\Delta^2} e^{-\frac{2\Omega}{\hbar v_F}R}, \tag{C7}$$

$$I_2 = \mathrm{Re}\int_{i\tilde{Q}}^{\infty+i\tilde{Q}} d\Omega \frac{i\Omega}{\sqrt{\Omega^2+\Delta^2}} e^{-\frac{2\Omega}{\hbar v_F}R}, \tag{C8}$$

$$I_3 = \mathrm{Re}\int_{i\tilde{Q}}^{\infty+i\tilde{Q}} d\Omega e^{-\frac{2\Omega}{\hbar v_F}R}. \tag{C9}$$

Consider the closed loop in the complex Ω plane as shown in Fig. 5 to calculate the three integrals, we can have

$$I_n = I_{n,C_1} + I_{n,0} + I_{n,C_2}, \tag{C10}$$

in which $n = 1, 2, 3$ and $I_{n,0}$ is the corresponding integral without supercurrent.

The line C_1 can be described as $\Omega = ib$ with $d\Omega = idb$ and integrate b from $\tilde{Q}$ to 0. The three integrals can be calculated as follows:

$$I_{1,C_1} = \mathrm{Re}\int_{C_1} d\Omega \frac{\Omega^2}{\Omega^2+\Delta^2} e^{-\frac{2\Omega}{\hbar v_F}R} = \mathrm{Re}\int_{\tilde{Q}}^0 idb \frac{(ib)^2}{(ib)^2+\Delta^2} e^{-\frac{2ib}{\hbar v_F}R} = \int_{\tilde{Q}}^0 db \frac{-b^2}{-b^2+\Delta^2} \sin\left(\frac{2bR}{\hbar v_F}\right) \approx 0, \tag{C11}$$

$$I_{2,C_1} = \mathrm{Re}\int_{C_1} d\Omega \frac{i\Omega}{\sqrt{\Omega^2+\Delta^2}} e^{-\frac{2\Omega}{\hbar v_F}R} = \mathrm{Re}\int_{\tilde{Q}}^0 idb \frac{i(ib)}{\sqrt{(ib)^2+\Delta^2}} e^{-\frac{2ib}{\hbar v_F}R} = \int_{\tilde{Q}}^0 db \frac{-b}{\sqrt{-b^2+\Delta^2}} \sin\left(\frac{2bR}{\hbar v_F}\right) \approx 0, \tag{C12}$$

$$I_{3,C1} = \mathrm{Re}\int_{C_1} d\Omega e^{-\frac{2\Omega}{\hbar v_F}R} = \mathrm{Re}\int_{\tilde{Q}}^0 idb e^{-\frac{2ib}{\hbar v_F}R} = \int_{\tilde{Q}}^0 db \sin\left(\frac{2bR}{\hbar v_F}\right) \approx 0. \tag{C13}$$

Here everything becomes zero because of the appearance of $\sin(\frac{bR}{\hbar v_F})$ in the integrands since $b \in [0, \tilde{Q}]$ and we take $\frac{\Delta R}{\hbar v_F} \to 0$ and therefore $\frac{\tilde{Q}R}{\hbar v_F} \to 0$ due to $\tilde{Q} < \Delta$.

The line C_2 can be described as $\Omega = a + ib$ with $d\Omega = idb$, $a \to +\infty$ and integrate b from 0 to $\tilde{Q}$. The three integrals can be calculated as follows:

$$I_{1,C_2} = \mathrm{Re}\int_{C_2} d\Omega \frac{\Omega^2}{\Omega^2+\Delta^2} e^{-\frac{2\Omega}{\hbar v_F}R} = \mathrm{Re}\lim_{a\to+\infty}\int_0^{\tilde{Q}} idb \frac{(a+ib)^2}{(a+ib)^2+\Delta^2} e^{-\frac{2(a+ib)}{\hbar v_F}R} = 0, \tag{C14}$$

$$I_{2,C_2} = \mathrm{Re}\int_{C_2} d\Omega \frac{i\Omega}{\sqrt{\Omega^2+\Delta^2}} e^{-\frac{2\Omega}{\hbar v_F}R} = \mathrm{Re}\lim_{a\to+\infty}\int_0^{\tilde{Q}} idb \frac{i(a+ib)}{\sqrt{(a+ib)^2+\Delta^2}} e^{-\frac{2(a+ib)}{\hbar v_F}R} = 0, \tag{C15}$$

$$I_{3,C_2} = \mathrm{Re}\int_{C_2} d\Omega e^{-\frac{2\Omega}{\hbar v_F}R} = \mathrm{Re}\lim_{a\to+\infty}\int_0^{\tilde{Q}} idb e^{-\frac{2(a+ib)}{\hbar v_F}R} = 0. \tag{C16}$$

Here everything becomes zero since $e^{-\frac{2aR}{\hbar v_F}}$ in the integrands becomes zero for $a \to +\infty$.

Therefore, the supercurrent Q doesn't introduce additional terms for $I_{1,2,3}$. The integrals are given by

$$I_1 = I_{1,0} = \mathrm{Re}\int_0^\infty d\Omega \frac{\Omega^2}{\Omega^2+\Delta^2} e^{-\frac{2\Omega}{\hbar v_F}R} = \frac{\hbar v_F}{2R} - \frac{\pi\Delta}{2}\cos\left(\frac{2R}{R_0}\right) - \Delta\sin\left(\frac{2R}{R_0}\right)\mathrm{Ci}\left(\frac{2R}{R_0}\right) + \Delta\cos\left(\frac{2R}{R_0}\right)\mathrm{Si}\left(\frac{2R}{R_0}\right)$$
$$\approx \frac{\hbar v_F}{2R} - \frac{\pi\Delta}{2}, \tag{C17}$$

$$I_2 = I_{2,0} = \mathrm{Re}\int_0^\infty d\Omega \frac{i\Omega}{\sqrt{\Omega^2+\Delta^2}} e^{-\frac{2\Omega}{\hbar v_F}R} = 0, \tag{C18}$$

$$I_3 = I_{3,0} = \mathrm{Re}\int_0^\infty d\Omega e^{-\frac{2\Omega}{\hbar v_F}R} = \frac{\hbar v_F}{2R}, \tag{C19}$$

in which $\mathrm{Ci}(x) = \int_0^x \frac{1-\cos t}{t} dt$ is the cosine integral and $\mathrm{Si}(x) = \int_0^x \frac{\sin t}{t} dt$ is the sine integral. The final step in Eq. (C17) is obtained by applying $\sin x \to 0$, $\cos x \to 1$, $\mathrm{Ci}(x)\sin x \to 0$, and $\mathrm{Si}(x) \to 0$ for $x \to 0$ with $x = R/R_0$ and $R_0 = \hbar v_F/\Delta$.

Now we turn to I_4. To calculate I_4, we make the further approximations for small $\tilde{Q}$:

$$[(\Omega + i\tilde{Q})^2 + \Delta^2]^{-\frac{1}{2}} \sim [\Omega^2 + \Delta^2 + 2i\Omega\tilde{Q}]^{-\frac{1}{2}} = \frac{1}{\sqrt{\Omega^2+\Delta^2}}\left(1 + \frac{2i\Omega\tilde{Q}}{\Omega^2+\Delta^2}\right)^{-\frac{1}{2}} \sim \frac{1}{\sqrt{\Omega^2+\Delta^2}}\left(1 - \frac{i\Omega\tilde{Q}}{\Omega^2+\Delta^2}\right), \tag{C20}$$

$$[(\Omega - i\tilde{Q})^2 + \Delta^2]^{-\frac{1}{2}} \sim [\Omega^2 + \Delta^2 - 2i\Omega\tilde{Q}]^{-\frac{1}{2}} = \frac{1}{\sqrt{\Omega^2+\Delta^2}}\left(1 - \frac{2i\Omega\tilde{Q}}{\Omega^2+\Delta^2}\right)^{-\frac{1}{2}} \sim \frac{1}{\sqrt{\Omega^2+\Delta^2}}\left(1 + \frac{i\Omega\tilde{Q}}{\Omega^2+\Delta^2}\right). \tag{C21}$$

Insert the above approximations, we have

$$\begin{aligned} I_4 &= \mathrm{Re}\int_0^\infty d\Omega \frac{\Delta^2}{\Omega^2+\Delta^2}\left[1 + \frac{\Omega^2\tilde{Q}^2}{(\Omega^2+\Delta^2)^2}\right]e^{-\frac{2\Omega R}{\hbar v_F}} \\ &= I_{4,0} + \mathrm{Re}\int_0^\infty d\Omega \frac{\Delta^2\Omega^2\tilde{Q}^2}{(\Omega^2+\Delta^2)^3}e^{-\frac{2\Omega R}{\hbar v_F}} \\ &= I_{4,0} + \frac{\tilde{Q}^2}{4\sqrt{\pi}\Delta}\mathrm{MeijerG}\left(\left\{-\frac{1}{2}\right\};\{\};\left\{0,\frac{1}{2},\frac{3}{2}\right\};\{\};\frac{R^2\Delta^2}{\hbar^2 v_F^2}\right), \end{aligned} \tag{C22}$$

$$\begin{aligned} I_{4,0} &= \mathrm{Re}\int_0^\infty d\Omega \frac{\Delta^2}{\Omega^2+\Delta^2}e^{-\frac{2\Omega R}{\hbar v_F}} = \Delta \mathrm{Ci}\left(\frac{2R}{R_0}\right)\sin\left(\frac{2R}{R_0}\right) + \frac{\Delta}{2}\cos\left(\frac{2R}{R_0}\right)\left[\pi - 2\mathrm{Ci}\left(\frac{2R}{R_0}\right)\right] \\ &\approx \frac{\pi\Delta}{2}, \end{aligned} \tag{C23}$$

in which $I_{4,0}$ is the result without supercurrent and the Meijer G-function is introduced using the syntax of Ref. [49]. Based on the above results, the difference between with and without supercurrent only comes from the Meijer G-function-related terms proportional to Q^2. We finally arrive at

$$E_{\mathrm{RKKY},0} = 2\pi^3 J^2 \frac{\pi R\Delta + (\pi R\Delta - \hbar v_F)\cos(2k_F R)}{R}, \tag{C24}$$

$$E_{\mathrm{RKKY}} = E_{\mathrm{RKKY},0} + \pi^{\frac{5}{2}} J^2 \frac{\tilde{Q}^2}{\Delta}\mathrm{MeijerG}\left(\left\{-\frac{1}{2}\right\};\{\};\left\{0,\frac{1}{2},\frac{3}{2}\right\};\{\};\frac{R^2\Delta^2}{\hbar^2 v_F^2}\right)\cos^2(k_F R), \tag{C25}$$

where the previous omitted constant proportional to J^2 is now included.

To ensure $\tilde{Q} < \Delta$, it is found that the supercurrent $Q < \frac{5.25\times10^{-4}}{a}$ for typical parameter values $\Delta = 1$ meV, $a = 0.1$ nm, and $k_F = 0.5/a$, which is much smaller than $Q \sim \frac{0.1}{a}$ for which we observe switching behavior using a numerical approach valid for arbitrary Q in the main text. Therefore, the analytical expression above for the RKKY interaction including supercurrent has a regime of validity which falls outside the range of Q values where switching is likely to be observable.

[1] A. Brataas, A. D. Kent, and H. Ohno, Current-induced torques in magnetic materials, Nat. Mater. **11**, 372 (2012).

[2] S. Shi, S. Liang, Z. Zhu, K. Cai, S. D. Pollard, Y. Wang, J. Wang, Q. Wang, P. He, J. Yu, G. Eda, G. Liang, and H. Yang, All-electric magnetization switching and Dzyaloshinskii–Moriya interaction in WTe_2/ferromagnet heterostructures, Nat. Nanotechnol. **14**, 945 (2019).

[3] K. Yamada, S. Kasai, Y. Nakatani, K. Kobayashi, H. Kohno, A. Thiaville, and T. Ono, Electrical switching of the vortex core in a magnetic disk, Nat. Mater. **6**, 270 (2007).

[4] K. C. Chun, H. Zhao, J. D. Harms, T. Kim, J. Wang, and C. H. Kim, A scaling roadmap and performance evaluation of in-plane and perpendicular MTJ based STT-MRAMS for high-density cache memory, J. Solid-State Circuits **48**, 598 (2013).

[5] B. Tudu and A. Tiwari, Recent developments in perpendicular magnetic anisotropy thin films for data storage applications, Vacuum **146**, 329 (2017).

[6] P. Li, J. Kally, S. S.-L. Zhang, T. Pillsbury, J. Ding, G. Csaba, J. Ding, J. S. Jiang, Y. Liu, R. Sinclair, C. Bi, A. DeMann, G. Rimal, W. Zhang, S. B. Field, J. Tang, W. Wang, O. G. Heinonen, V. Novosad, A. Hoffmann *et al.*, Magnetization switching using topological surface states, Sci. Adv. **5**, eaaw3415 (2019).

[7] S. Fukami, C. Zhang, S. DuttaGupta, A. Kurenkov, and H. Ohno, Magnetization switching by spin–orbit torque in an antiferromagnet–ferromagnet bilayer system, Nat. Mater. **15**, 535 (2016).

[8] C. K. Safeer, E. Jué, A. Lopez, L. Buda-Prejbeanu, S. Auffret, S. Pizzini, O. Boulle, I. M. Miron, and G. Gaudin, Spin–orbit

torque magnetization switching controlled by geometry, Nat. Nanotechnol. **11**, 143 (2016).
[9] Y. Fan, P. Upadhyaya, X. Kou, M. Lang, S. Takei, Z. Wang, J. Tang, L. He, L.-T. Chang, M. Montazeri, G. Yu, W. Jiang, T. Nie, R. N. Schwartz, Y. Tserkovnyak, and K. L. Wang, Magnetization switching through giant spin–orbit torque in a magnetically doped topological insulator heterostructure, Nat. Mater. **13**, 699 (2014).
[10] C. Sun, J. Deng, S. M. Rafi-Ul-Islam, G. Liang, H. Yang, and M. B. A. Jalil, Field-free switching of perpendicular magnetization through spin Hall and anomalous Hall effects in ferromagnet–heavy-metal–ferromagnet structures, Phys. Rev. Appl. **12**, 034022 (2019).
[11] F. Matsukura, Y. Tokura, and H. Ohno, Control of magnetism by electric fields, Nat. Nanotechnol. **10**, 209 (2015).
[12] J. Linder and J. W. A. Robinson, Superconducting spintronics, Nat. Phys. **11**, 307 (2015).
[13] M. Eschrig, Spin-polarized supercurrents for spintronics: A review of current progress, Rep. Prog. Phys. **78**, 104501 (2015).
[14] R. S. Keizer, S. T. B. Goennenwein, T. M. Klapwijk, G. Miao, and A. Gupta, A spin triplet supercurrent through the half-metallic ferromagnet CrO_2, Nature (London) **439**, 825 (2006).
[15] J. W. A. Robinson, J. D. S. Witt, and M. G. Blamire, Controlled injection of spin-triplet supercurrents into a strong ferromagnet, Science **329**, 59 (2010).
[16] T. S. Khaire, M. A. Khasawneh, W. P. Pratt, and N. O. Birge, Observation of spin-triplet superconductivity in Co-based Josephson junctions, Phys. Rev. Lett. **104**, 137002 (2010).
[17] A. Singh, C. Jansen, K. Lahabi, and J. Aarts, High-quality CrO_2 nanowires for dissipation-less spintronics, Phys. Rev. X **6**, 041012 (2016).
[18] X. Waintal and P. W. Brouwer, Magnetic exchange interaction induced by a Josephson current, Phys. Rev. B **65**, 054407 (2002).
[19] E. Zhao and J. A. Sauls, Theory of nonequilibrium spin transport and spin-transfer torque in superconducting-ferromagnetic nanostructures, Phys. Rev. B **78**, 174511 (2008).
[20] J. Linder and T. Yokoyama, Supercurrent-induced magnetization dynamics in a Josephson junction with two misaligned ferromagnetic layers, Phys. Rev. B **83**, 012501 (2011).
[21] A. Buzdin, Direct coupling between magnetism and superconducting current in the Josephson φ_0 junction, Phys. Rev. Lett. **101**, 107005 (2008).
[22] S. Teber, C. Holmqvist, and M. Fogelström, Transport and magnetization dynamics in a superconductor/single-molecule magnet/superconductor junction, Phys. Rev. B **81**, 174503 (2010).
[23] C. Holmqvist, S. Teber, and M. Fogelström, Nonequilibrium effects in a Josephson junction coupled to a precessing spin, Phys. Rev. B **83**, 104521 (2011).
[24] I. Kulagina and J. Linder, Spin supercurrent, magnetization dynamics, and φ-state in spin-textured Josephson junctions, Phys. Rev. B **90**, 054504 (2014).
[25] K. M. D. Hals, Supercurrent-induced spin-orbit torques, Phys. Rev. B **93**, 115431 (2016).
[26] D. S. Rabinovich, I. V. Bobkova, A. M. Bobkov, and M. A. Silaev, Resistive state of superconductor-Ferromagnet-superconductor josephson junctions in the presence of moving domain walls, Phys. Rev. Lett. **123**, 207001 (2019).
[27] I. V. Bobkova, A. M. Bobkov, I. R. Rahmonov, A. A. Mazanik, K. Sengupta, and Y. M. Shukrinov, Magnetization reversal in superconductor/insulating ferromagnet/superconductor Josephson junctions on a three-dimensional topological insulator, Phys. Rev. B **102**, 134505 (2020).
[28] M. A. Ruderman and C. Kittel, Indirect exchange coupling of nuclear magnetic moments by conduction electrons, Phys. Rev. **96**, 99 (1954).
[29] T. Kasuya, A Theory of metallic ferro- and antiferromagnetism on Zener's model, Prog. Theor. Phys. **16**, 45 (1956).
[30] K. Yosida, Magnetic Properties of Cu-Mn Alloys, Phys. Rev. **106**, 893 (1957).
[31] J. Bardeen, L. N. Cooper, and J. R. Schrieffer, Theory of superconductivity, Phys. Rev. **108**, 1175 (1957).
[32] N. E. Alekseevskii, I. A. Garifullin, B. I. Kochelaev, and E. G. Kharakhash'yan, Electron spin resonance on localized magnetic states in the superconducting system La-Er, Zh. Eksp. Teor. Fiz. **72**, 1523 (1977) [JETP **45**, 799 (1977)].
[33] B. Kochelaev, L. Tagirov, and M. Khusainov, Spatial dispersion of spin susceptibility of conduction electrons in a superconductor, Zh. Eksp. Teor. Fiz. **76**, 578 (1979) [JETP **49**, 578 (1979)].
[34] M. Khusainov, Indirect RKKY exchange and magnetic states of ferromagnet-superconductor superlattices, Zh. Eksp. Teor. Fiz. **109**, 524 (1996) [JETP **82**, 278 (1996)].
[35] D. N. Aristov, S. V. Maleyev, and A. G. Yashenkin, RKKY interaction in layered superconductors with anisotropic pairing, Z. Phys. B: Condens. Matter **102**, 467 (1997).
[36] M. Tinkham, *Introduction to Superconductivity* (Dover Books on Physics Series, Dover, New York, 2004).
[37] R. Takashima, Y. Kato, Y. Yanase, and Y. Motome, Generation and control of noncollinear magnetism by supercurrent, Phys. Rev. B **97**, 081107 (2018).
[38] A. M. Black-Schaffer and J. Linder, Strongly anharmonic current-phase relation in ballistic graphene Josephson junctions, Phys. Rev. B **82**, 184522 (2010).
[39] A. Yazdani, B. A. Jones, C. P. Lutz, M. F. Crommie, and D. M. Eigler, Probing the local effects of magnetic impurities on superconductivity, Science **275**, 1767 (1997).
[40] L. Yu, Bound state in superconductors with paramagnet impurities, Acta Phys. Sin. **21**, 75 (1965).
[41] H. Shiba, Classical spins in superconductors, Prog. Theor. Phys. **40**, 435 (1968).
[42] A. I. Rusinov, On the theory of gapless superconductivity in alloys containing paramagnetic impurities, Zh. Eksp. Teor. Fiz. **56**, 2047 (1969) [Sov. Phys. JETP **29**, 1101 (1969)].
[43] K. Akkaravarawong, J. I. Väyrynen, J. D. Sau, E. A. Demler, L. I. Glazman, and N. Y. Yao, Probing and dressing magnetic impurities in a superconductor, Phys. Rev. Res. **1**, 033091 (2019).
[44] M. N. Gastiasoro and B. M. Andersen, Enhancing superconductivity by disorder, Phys. Rev. B **98**, 184510 (2018).
[45] L. N. Bulaevskii and S. V. Panyukov, RKKY interaction in metals with impurities, Pis'ma Zh. Eksp. Teor. Fiz. **43**, 190 (1986) [JETP Lett. **43**, 240 (1986)].
[46] F. Kuster, S. Brinker, S. Lounis, S. S. P. Parkin, and P. Sessi, Long range and highly tunable interaction between local spins

coupled to a superconducting condensate, Nat. Commun. **12**, 6722 (2021).

[47] K. V. Samokhin and M. B. Walker, Effect of magnetic field on impurity bound states in high-T_c superconductors, Phys. Rev. B **64**, 024507 (2001).

[48] J. A. Ouassou, T. Yokoyama, and J. Linder, RKKY interaction in triplet superconductors: Dzyaloshinskii-Moriya-type interaction mediated by spin-polarized Cooper pairs, Phys. Rev. B **109**, 174506 (2024).

[49] https://www.mathworks.com/help/symbolic/meijerg.html